Suppressed cavitation in die-drawn isotactic polypropylene

Dong Lyu,[1,2] Yingying Sun,[3] Ying Lu,[1,] Lingzhi Liu,[1] Ran Chen,[1] Glen Thompson,[4] Philip Caton-Rose,[4] Phil Coates,[4] Yan Wang,[5] Yongfeng Men.[1,2,*]*

[1] State Key Laboratory of Polymer Physics and Chemistry, Changchun Institute of Applied Chemistry, Chinese Academy of Sciences, Renmin Street 5625, Changchun 130022, P. R. China

[2] University of Science and Technology of China, Hefei 230026, P. R. China

[3] ExxonMobil Asia Pacific Research & Development Co., Ltd., 1099 Zixing Road, Minhang District, Shanghai 200241, P. R. China

[4] Polymer Interdisciplinary Research Centre, University of Bradford, Bradford BD7 1DP, UK

[5] Key Laboratory of High Performance Plastics (Jilin University), Ministry of Education, National & Local Joint Engineering Laboratory for Synthesis Technology of High Performance Polymer, College of Chemistry, Jilin University, Changchun, 130012, P. R. China

KEYWORDS: cavitation, die drawing, deformation, isotactic polypropylene, X-ray, beta iPP.

ABSTRACT

Cavitation is an important phenomenon in solid phase deformation of polymers, with either potential adverse effects on physical properties or creating potential opportunities for new properties. In either case, it needs to be better understood to help achieve better control of cavitation and its effects. Cavitation associated with solid phase deformation in a β-nucleated isotactic polypropylene was found to depend on the solid phase deformation route employed. Compared with samples obtained by free tensile stretching, cavitation was suppressed in samples deformed via die drawing, although an almost identical β to α phase transition was observed for both deformation routes. Even when die-drawn samples were subsequently deformed to large strains by free stretching, there was still no comparable cavitation compared with the single free tensile-stretching route. The die-drawing process appears to suppress cavitation by fundamentally diminishing the amount of growable nuclei of cavities, rather than merely hindering the growth of cavities. A relationship between cavitation intensity and the fractions of lamellae along specific directions has been established. During subsequent free stretching of die drawn samples, newly-created cavities were suggested to be initiated within the crystalline layers. The reduction of the cavity-nuclei in the die-

drawing process originated from the stabilization of the connections between the crystalline blocks within the lamellae.

1. Introduction

Cavitation, as a competitor of plastic flow[1, 2] during the deformation of semi-crystalline polymer materials, could drastically influence product properties during service. For example, the existence of cavitation could compromise transparency and mechanical performance, or even lead to the final failure of products.[2-6] However, materials with carefully controlled cavitation could serve as battery separators, sound insulators, or shock resistance components.[7-12] Intended triggering of cavitation (but around inert fillers) has been used to decrease the density of a filled polymer in die drawing, to obtain structural products with controlled stiffness and strength, but with light weight.[13] It is essential to understand the formation as well as the control of cavitation behavior. The relationships between the cavitation and the thermal history of the material, deformation temperature, as well as strain rate have been well-established[1, 5, 14-17]. In addition to these deformation parameters, deformation routes also significantly influence the cavitation behavior of semi-crystalline polymers.

Cavitation has normally been observed in tensile stretching, rarely in solid-state shearing and never in compression.[1, 3, 18, 19] Galeski *et al,*[3] comparing sheared and tensile stretched isotactic polypropylene (iPP) samples, concluded that there had to be a certain

negative stress to initiate and sustain cavitation. Due to the compressive component of stress, no cavitation could be formed for samples deformed via channel die compression. Earlier, Aboulfaraj *et al* [18] investigated the deformation behavior of iPP possessing α or β form spherulites during both shearing and stretching. They observed that cavitation in the samples with α spherulites could only be found during stretching, while for the ones with β spherulites both shearing and stretching could initiate the cavitation. It should be noted that the β form iPP transforms to the α form during deformation at relatively high temperature,[20, 21] and this process is often accompanied by cavitation.[9, 20, 22]

Die drawing is a widely applied solid-state polymer processing technique.[13, 23-25] In this process, a billet of polymer is pulled out of a carefully designed, normally convergent angle die. The polymer billet undergoes compression, shearing and, normally predominantly, elongation. Cavitation has occasionally been observed in die-drawn samples distant from the die.[25, 26] However, previous studies mainly focus on the enhanced mechanical behavior of the die-drawn samples, with no discussion on cavitation.

To help understand the cavitation behavior of die-drawn products, an iPP compounded with β-nucleating agents was employed. Ultra-small angle X-ray scattering (USAXS) was used to investigate voids inside die-drawn and tensile free drawn samples. The results indicate that cavitation is suppressed in die-drawn products,

compared with samples deformed via tensile stretching and die drawing. When further deforming the die-drawn samples via free tensile stretching, the cavitation phenomenon became more evident, but still weaker than that of the sample deformed only via tensile stretching. Based on the observed cavitation intensity and direction, the reason for the suppressed cavitation in the die-drawn sample is deduced and the possible nucleation sites of the cavities are suggested.

2. Experimental section

2.1 Material information and sample preparation

A commercial iPP with a molecular weight M_w= 158 900 g mol^{-1} and a polydispersity (M_w/ M_n) 3.8 provided by ExxonMobil was used for this investigation. To alter the initial microstructure of the samples, a β-nucleating agent TMB-5 (N, N'-Dicyclohexylterephthalamide) was employed, supplied by Chemical Institute of Shanxi, China. To avoid thermal decay, two antioxidants, Pentaerythtieol tetrakis(3,4-di-tert-butyl-4-hydroxyhydrocinnamate) and Tris(2,3-diitertibutylphenyl) phosphite, both from Sigma-Aldrich, were blended into the polymer melt with the nucleating agents. The weight ratio for the polymer melt and additives was 1000/1/1/1. After full mixing, the polymer was injection molded by ExxonMobil into tensile bars. Injection moulded samples were then cut into billets of dimensions of 5 mm*4 mm*170 mm for die drawing and tensile stretching studies.

2.2 Deformation tests

Three routes of deformation were explored: (a) free tensile drawing; (b) die drawing; (c) free tensile drawing of samples cut from die drawn products produced by route (b). A sketch depicting all deformation processes is shown in Figure 1.

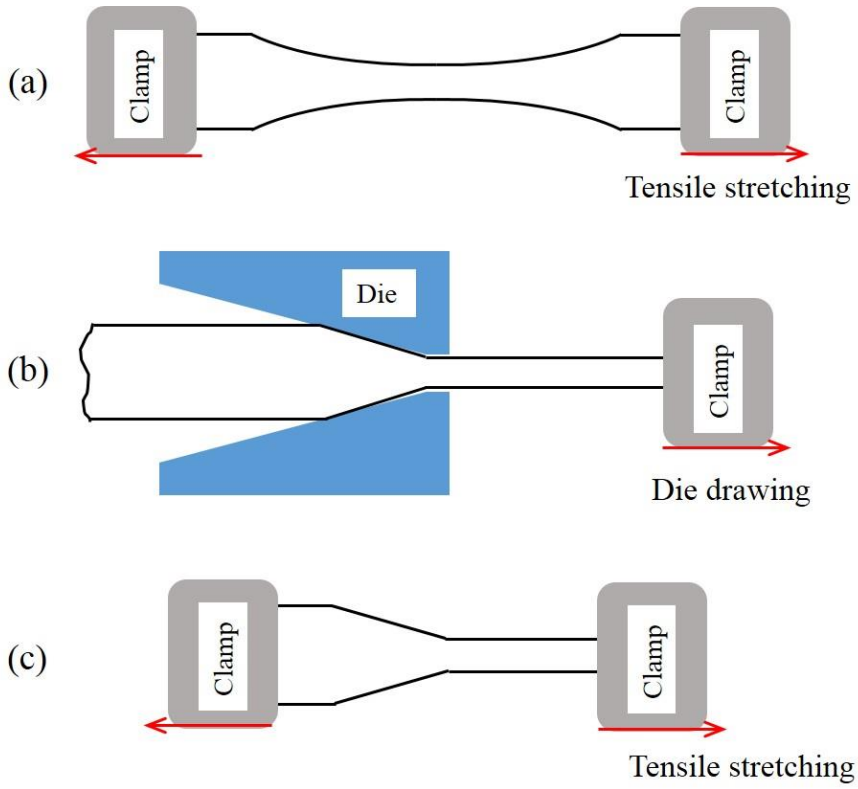

Figure 1. A schematic diagram corresponding to each deformation process. (a) An already necked sample deformed via tensile stretching, (b) the die drawing process, (c) free drawing of the die-drawn sample.

(a) Free tensile drawing: An electronic universal testing machine (Instron 5869, Instron, USA) equipped with heating oven was used to free tensile stretch the as-cut injection moulded samples which were 5 mm in width and 4 mm in thickness, at 130

ºC and 140 ºC. The initial gauge length was 20 mm and the elongation speed was 94 mm/min.

(b) Die drawing: Die-drawing tests were accomplished by using a self-designed mini die-drawing facility using a converging die with exit dimension of 5 mm*2 mm, the details of which could be found in a previous study.[27] Samples were die drawn at the same temperatures and speed as the free drawing tests?.

Both die drawn and free tensile stretched samples were deformed to an extent that a portion of the bars remained outside of the neck or had not passed through the die. Consequently, specimens with a distribution of local axial strain from the almost undeformed state to the most highly deformed state were obtained.

(c) Free tensile drawing of die drawn samples: Several die-drawn samples were further free tensile stretched by another universal electromechanical testing machine (AG-I 20kN, Shimadzu, Japan) at the same conditions. During this second stage deformation of the die drawn samples, the initial gauge length was set as 20 mm covering the entire region previously located within the die. Thus, the second stage free stretching of the die drawn samples started with an asymmetric shape with one side being nearly undeformed (including material which had just entered the convergent die), then a portion that was previously within the die region so having an axial strain gradient, to another portion that had been fully processed by die drawing to an approximately constant value of the selected high strain. These die drawn samples were

then stretched to different overall engineering elongations of 25%, 50%, 100% in the second stage free stretching at temperature…?. The samples are designated as D25%T, D50%T and D100%T samples in the following discussion. Due to the existing strain gradient along the gauge length of the die drawn samples, deformation in second free stretching tests occurred mainly in the previously less deformed portion.

The apparent local draw ratio, R_A, at any point along the axis of specimens, was calculated based on the local cross-sectional area of samples before and after deformation:[23]

$$R_A = \frac{\textit{Original billet cross-sectional area}}{\textit{Final billet cross-sectional area}} \quad (1)$$

To evaluate the local draw ratio precisely, a high resolution camera was used to capture the variation of the cross-sectional area, with the sample width and thickness measured every 0.5 mm throughout the whole sample. Prior to the second stage deformation of die-drawn samples, these were marked at regular positions. The shape change at these specific positions during the second stage deformation, could be calculated by the corresponding cross-sectional area of the die-drawn sample before and after the second stage deformation. So, the local draw ratio with respect to the original undeformed sample is designated as R_A^o, whereas the local draw ratio during the second stage deformation is labelled as R_A^d since the calculation of the local draw

ratio during the second deformation is related to the sample dimensions after the die-drawing process.

2.3 X-ray experiments

Micro-focus wide-angle X-ray diffraction (WAXD) was employed to investigate the crystalline phase transition as well as the lamellae distribution of the deformed samples. The facility consists of Genix 3D X-ray generator equipped with a focusing mirror (GeniX^{3D}, Xenocs SA, France) and a Pilatus 100K detector (487 pixels*197 pixels, pixel size=172*172 μm^2, DECTRIS, Swiss). The sample to detector distance was 50 mm and the beam size at the sample position was 60*40 μm^2. The samples were moved along their elongation direction, with a step interval of 0.5 mm after each acquisition time of 60 s. The 1D diffraction curves were obtained by integrating the collected 2D WAXD patterns over the whole azimuthal angles to account for scattering intensities of crystals with different orientations. The 1D diffraction curves were composed of both sharp characteristic peaks for the α and β crystalline phases and one broad amorphous peak. By fitting these peaks with several Gaussian functions, the area of each peak could be readily obtained and subsequently the fractions of the β crystalline phase as well as the α crystalline phase could be determined.[28, 29] For each curve the fitting procedure was repeated at least three times to gain a better accuracy.

Ultra-small angle X-ray scattering (USAXS) experiments were performed to evaluate cavitation behaviour, using a customized Xeuss X-ray apparatus (Xenocs SA, France) for which the X-ray generator and the detector were the same as the ones for micro-focus X-ray diffraction. A mirror that produces quasi-parallel X-ray beam was used. The sample-to-detector distance was 6487 mm. The beam size at the sample position was 0.6*0.6 mm^2 shaped by two sets of scatterless slits systems located 2.4 m apart from each other. The acquisition time for each 2D USAXS pattern was 600 s. A semiconductor diode was employed to record and normalize the X-ray intensity.

The integrated scattering intensity, also named the scattering invariant, Q, is defined as:[30]

$$\mathrm{Q} \propto \int_{q_{min}}^{q_{max}} \int_{q_{min}}^{q_{max}} I(q_x,\, q_y)\, dq_x\, dq_y \qquad (2)$$

Q reflects the scattering contributions of every scattering component inside the system and it is related to the volume fractions of scattering components as well as the electron density difference between them. To compare the scattering invariant Q of samples at different strains, the obtained scattering intensity distribution needs to be corrected by considering changes in scattering volume caused by the progressive thinning of the samples at larger strains. Changes in the sample thickness would cause different absorption of the X-ray and consequently influence the actual X-ray intensity being scattered during the experiments. Hence a semiconductor diode was put directly after

the sample to measure the X-ray flux remaining, after passing through the samples. This remaining X-ray flux could serve as an indicator to normalize $I(q_x, q_y)$ in Equation 2. Each USAXS pattern was first normalized by the corresponding X-ray flux after absorption. After background subtraction, the normalized Q could be obtained by integrating half of the pattern (from 0° to 180°).

The dimensions of cavities were evaluated based on the model proposed by Fischer *et al.*[31] In this model, the voids are simplified as randomly distributed cylinders with heights along the elongation direction:

$$I(q_r, q_h) \propto \iint_0^\infty R^4 H^2 \left[\frac{2J_1(q_r R)}{q_r R}\right]^2 \left[\frac{\sin(q_h H/2)}{q_h H/2}\right]^2 D(R,H)\, dR\, dH \quad (3)$$

When the radius R and heights H of the cylinders are not correlated, the above equation can be further simplified as:

$$I(q_r, q_h) \propto \int_0^\infty R^4 \left[\frac{J_1(q_r R)}{q_r R}\right]^2 D_1(R)\, dR \times \int_0^\infty H^2 \left[\frac{\sin(q_h H/2)}{q_h H/2}\right]^2 D_2(H)\, dH \quad (4)$$

where the $D_1(R)$ and $D_2(H)$ are the size distribution of the radius and the height, which are considered as log-normal distributions. This model ignores misalignments/tilting of the cylinders which is not strictly accurate. Therefore, for SAXS patterns showing scattering intensity distributions of structures having considerable deviation from perfect orientation were then not fitted.

The typical size of the cavities was also checked by scanning electron microscopy (SEM) experiments via a field emission ESEM setup (Philips-FEI XL-30 ESEM). In order to measure the inside microstructure of the samples by ESEM, the samples were quenched into liquid nitrogen and left for at least ten minutes before they were fractured to create fresh inner surfaces. The prepared samples were coated with gold prior to the SEM experiments.

3. Results and Discussion

3.1. Suppressed cavitation in die-drawn sample

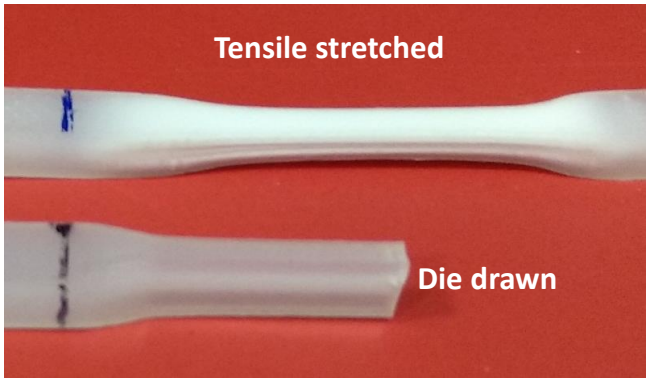

Figure 2. A photograph of samples deformed either via tensile stretching or die drawing. (Deformation temperature 130 ºC)

A photograph of the as deformed tensile-stretched sample and die-drawn sample is shown in Figure 2. Strong stress-whitening is observed in the tensile-stretched sample, but only slight whitening is observed in the die-drawn sample. The stress-whitening behavior is essentially related to micro voids produced in the polymer matrix.

Cavities scatter visible light when their sizes are comparable to the wave length of visible light, making the original near transparent polymer matrix appear white.[17] As this whitening phenomenon can be directly observed by eye, it is often used as a qualitative indicator of cavitation. The different extent of whitening of samples can be linked to different degrees of cavitation. To confirm that the cavitation was actually different between samples deformed via different methods, scanning USAXS measurements were performed over different positions of the samples, to observe structural characteristics at different extents of deformation. The corresponding 2D USAXS patterns are shown in Figure 3.

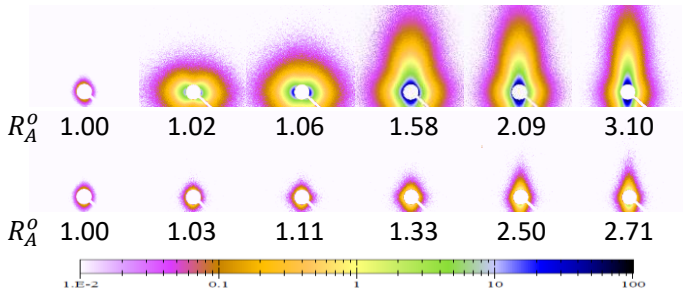

Figure 3. Selected 2D scanning USAXS patterns of the tensile-stretched sample (top) and the die-drawn sample (bottom). Elongation direction: horizontal.

In the undeformed state, e.g. the first pattern in both the top row (patterns for tensile-stretched samples) and the bottom row (patterns for die-drawn samples), only a slight and blurred scattering signal could be found near the beam stop. This may be due to structures induced during the injection molding process or additives of large dimension. USAXS scans were made of the free tensile stretched and die drawn samples, from their

undeformed region to their highly deformed regions, i.e. passing through the neck or portion previously within the die respectively. For the tensile-stretched sample, an intense signal abruptly appeared near the beam stop. The scattering signal first occurred horizontally (e.g. at R_A^0=1.02) and then vertically in the 2D USAXS patterns, indicating the orientation direction of the cavities had changed. Similar to other investigations,[3, 15, 32] cavities were perpendicular to the deformation direction at their first appearance, but rearranged along the deformation direction upon stretching. In the case of the die-drawn sample, new scattering signals were observed after deformation, but their intensity was not comparable to those of the tensile-stretched sample. Unlike the tensile-stretched sample, there was no rearrangement of the direction of cavities in the die-drawn sample. The cavities were already oriented along the elongation direction once they appeared. Both the scattering intensity difference and the modes of evolution of the cavities indicated that the cavitation was affected by the route of deformation.

According to previous studies, the β form iPP either transforms to the mesophase at low temperatures or to the α phase at elevated temperatures during deformation.[33] In this work, no mesophase could be traced since the deformation temperature was relatively high. Also, deformation of the β form iPP is often accompanied by cavitation in the system. Some researchers believed that voids originate from the volume contraction during the transition from the β phase to the α phase of iPP,[20, 22] while others consider that it is the nature of the β form iPP to initiate cavitation under deformation.[9,

[32, 34] Based on either of the above two theories, the cavitation should be related to the fraction of β phase. Hence, WAXD experiments were performed to determine the evolution of the β phase upon deformation. Selected 1D WAXD curves and the evolution of each component during deformation are shown in Figure 4.

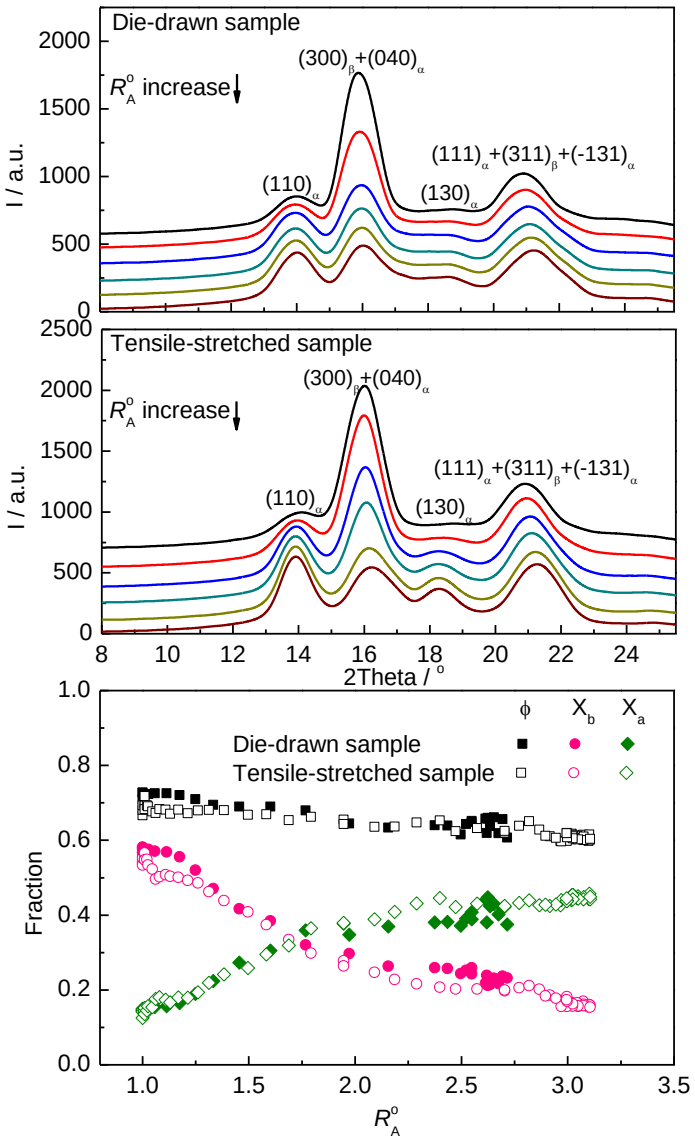

Figure 4. Selected 1D WAXD curves of the die-drawn sample (top), tensile-stretched sample (middle) and the evolution of the α phase, the β phase and the crystallinity in samples deformed by tensile stretching or die drawing (bottom).

During deformation, the β form gradually transforms to the α phase, as evidenced by the decrease of the fraction of the β form and the increase of α form shown in Figure 4. The crystallinity did not decrease significantly. In Figure 4, solid points (representing the die-drawn sample) almost overlay on the hollow points (representing the tensile-stretched sample), indicating both the phase transition behavior and the fractions of the β phase are determined by the extent of deformation only, irrespective of the route of deformation. Thus, the observed difference in extent of cavitation should not originate from the β to α phase transition of iPP alone, it is more of the influence of the route of deformation rather than the polymer matrix itself. The die-drawing process appears to suppress cavitation behaviour compared with the free tensile stretching.

3.2. Reason for suppression

In our previous work, the cavitation phenomenon was considered to be a three-step process: (I) the nucleation of cavities, (II) the growth of the already formed nuclei, and finally (III) stabilization of the cavities.[17, 35] Compression of material contacting the die during the initial part of die-drawing would be expected to limit the development of cavities. But did the difference between tensile-stretched sample and the die-drawn

sample originate merely from the confined development of cavities (step II)? Or more fundamentally, is the number of growable cavity nuclei reduced (step I)? These questions can be addressed by subsequent free stretching of die-drawn samples.

If the difference in cavitation is only a result of the restriction of cavity development induced by the die, further deformation without the die could be able to give enough space for the nuclei to grow. The already formed nuclei of cavities could develop drastically during subsequent free tensile stretching. Then similar or even more intensive cavitation could be found in the further stretched die-drawn sample. Based on this conjecture, three die-drawn samples were further free stretched to different overall elongation ratios, namely, the D25%T, D50%T and D100%T samples described in the experimental section.

When inspecting the second stage free stretched samples, interesting shape changing behaviour was observed in the samples. The detailed evolution of the local draw ratio, $R_{\mathrm{A}}^{\mathrm{o}}$, which was calculated based on the original sample cross-sectional area, on dependence of the distance to the die entrance, *X*, is shown in Figure 5. The die entrance and the die exit positions are indicated for each sample. The $R_{\mathrm{A}}^{\mathrm{d}}$ at the die entrance and exit was marked out as well, which represented the local draw ratio induced during the second stage deformation, at the corresponding position.

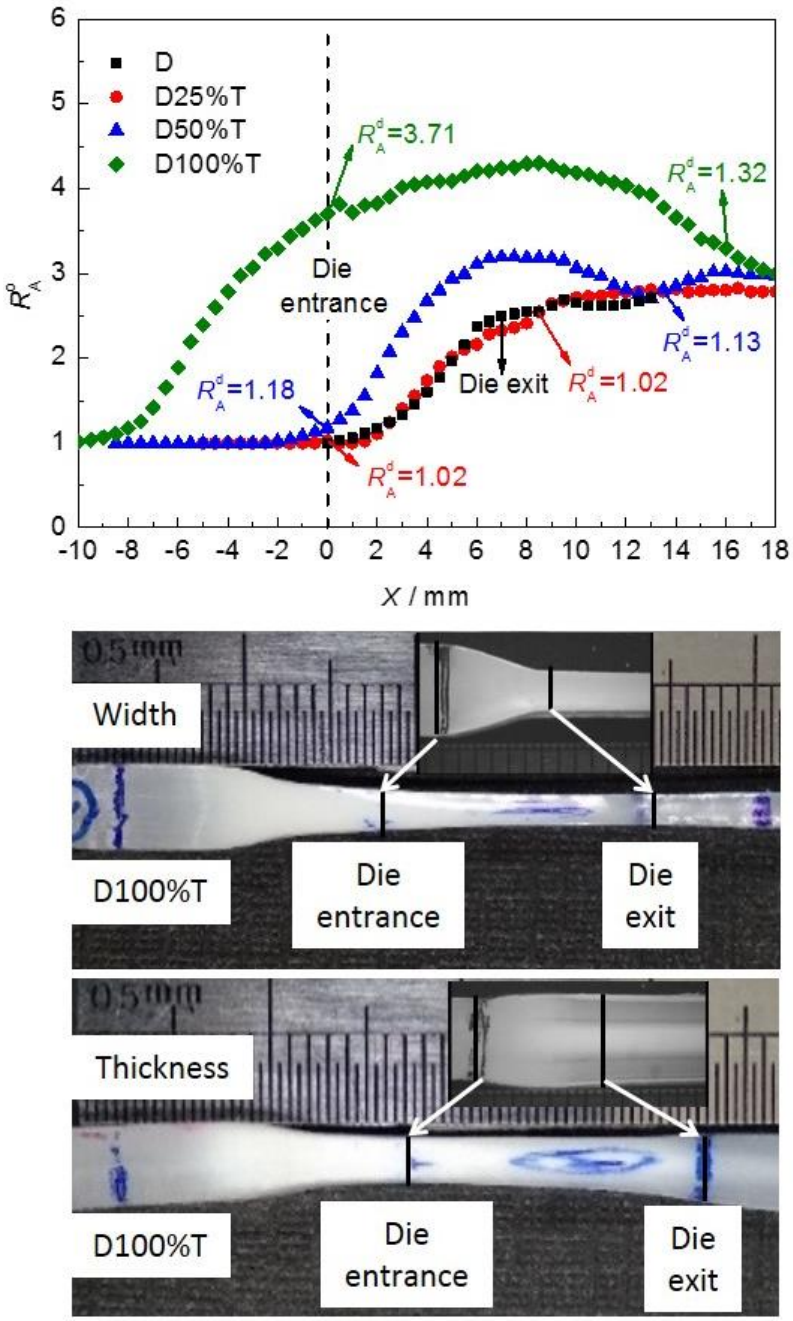

Figure 5. The draw ratio (R_A^o) distribution along the deformation direction of samples. *X*: the distance between the corresponding positions to the die entrance along the deformation direction. Bottom photos show shape change of the exemplar D100%T sample before and after second stage free stretching.

Unlike the die-drawn sample and the D25%T one, $R_{\mathrm{A}}^{\mathrm{o}}$ did not increase monotonically with *X* from the die entrance toward the die exit for the D50%T and D100%T samples. In these samples, the largest $R_{\mathrm{A}}^{\mathrm{o}}$ occurs in a location between the die entrance and the die exit. This phenomenon is a result of second stage free stretching of samples with an asymmetric distribution of deformation ratio induced by the die-drawing process. Although the die-drawing process reduces the cross-sectional area of a product, which leads to a larger true stress applied on the deformed part of the die-drawn sample during the second stage free stretching, the already deformed part tends not to further deform due to higher strain hardening in the more highly strained region of the sample. Rather, the less deformed portion, namely material which was originally near the die entry region, is more likely to deform as a result of its lower orientation. Therefore, during the second stage free stretching the largest $R_{\mathrm{A}}^{\mathrm{d}}$ occurs in a location of the sample which had originally been between the die entrance and the die exit.

The cross-sectional area of a simple convergent die-drawn sample should decrease from the convergent die entrance to the die exit, as a result of the deformation imposed by the die. But as discussed above, the largest $R_{\mathrm{A}}^{\mathrm{d}}$ appeared somewhere in between the die entrance and the die exit of the samples undergoing second stage free stretching. In other words, the $R_{\mathrm{A}}^{\mathrm{d}}$ would first increase and then decrease along the sample from the die entrance toward the die exit position. Consequently, the R_A^o at different positions

of the D25%T, D50%T and D100%T samples should be partially determined by the $R_{\mathrm{A}}^{\mathrm{d}}$.

For the D25%T sample, the second stage deformation, $R_{\mathrm{A}}^{\mathrm{d}}$ incurred was not large enough to disrupt the deformation pattern induced by the die-drawing process. Hence $R_{\mathrm{A}}^{\mathrm{o}}$ for this sample kept increasing as per the initial die-drawn sample. However, for the D50%T and D100%T samples, where a larger $R_{\mathrm{A}}^{\mathrm{d}}$ was induced during the second stage free stretching, a region in between the die entrance and the die exit would achieve the largest $R_{\mathrm{A}}^{\mathrm{o}}$, beyond which the effect of the second free stretching would gradually decline. At the positions closer to the die exit of the D50%T sample, the effect of second stage stretching $R_{\mathrm{A}}^{\mathrm{d}}$ almost disappeared, and $R_{\mathrm{A}}^{\mathrm{o}}$ increased again following the pattern induced during die drawing. But for the D100%T sample, the effect of the $R_{\mathrm{A}}^{\mathrm{d}}$ was so strong that the original pattern of $R_{\mathrm{A}}^{\mathrm{o}}$ for die drawing was overridden. As a consequence, $R_{\mathrm{A}}^{\mathrm{o}}$ for this sample kept reducing beyond its largest value at $X \sim 8.5$ mm.

The selected scanning 2D USAXS patterns of D25%T, D50%T and D100%T samples are shown in Figure 6, arranged top to bottom respectively. In accordance with $R_{\mathrm{A}}^{\mathrm{o}}$ evolution in Figure 5, $R_{\mathrm{A}}^{\mathrm{o}}$ did not keep increasing from die entrance to die exit for the D50%T and D100%T samples. 2D WAXD patterns at the corresponding positions are also included to reflect the differences in morphology in these samples. Clearly, the WAXD patterns at the die entrance positions of these samples are highly dependent on the second stage free tensile stretching. The major characteristic peaks in the D25%T

sample belonged to the β form, while these peaks are nearly consumed and replaced by the reflection peaks of the α form in the D100%T sample. With respect to the D50%T sample, the situation at the die entrance was similar to the one of D25%T sample while a more intensive transition from β to α phase could be observed in the former, at the positions beyond the die entrance. These observations reveal that the breakage of original crystallites and recrystallization of new lamellae gradually increase with increasing second stage deformation, i.e. from the D25%T sample to the D100%T sample.

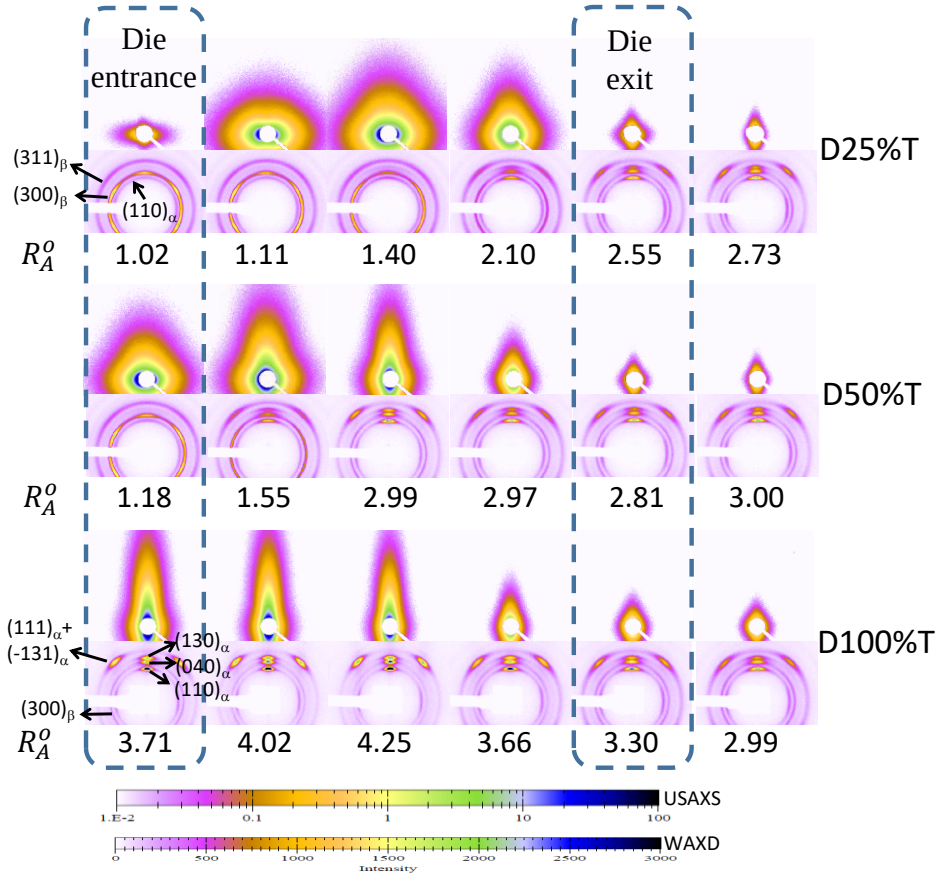

Figure 6. Selected 2D USAXS and WAXD patterns of die-drawn samples after second stage free stretching. Elongation direction: horizontal.

Comparing the USAXS patterns of these samples at the die entrance, it is clear that the cavitation behavior strongly depends on the extent of the second stage deformation. For the D25%T sample, the long axis of cavities is perpendicular to the elongation direction at the die entrance position. For the D100%T sample, the long axis of cavities is already along the elongation direction. The cavities in both the D25%T and D100%T samples exhibited a strong degree of orientation as evidenced by the sharp and narrow scattering streaks. On the other hand, the cavities in the D50%T sample were not oriented along one particular direction. The coexistence of both horizontal and vertical scattering signals blurs the 2D USAXS pattern of the D50%T sample. This represents an intermediate state of a rearrangement of orientation of cavities during tensile deformation, similar to that shown in Figure 3. All the samples shared the same microstructure after the die-drawing process and the further stretching conditions were identical. Hence the observed complex cavitation behaviour comes from the second stage free stretching.

We noticed the cavities would realign themselves with long axis along the elongation direction at the die entrance in the D50%T and D100%T samples, as compared to the D25%T one. This reorientation was complete in the D100%T sample, and thus no horizontal scattering streaks were observed. Such reorientation can be interpreted as a result of reborn lamellae with their normal along the deformation direction.[36] Mechanical melting and recrystallization generally take place during necking. The

location in the sample with R_A^o= 3.71 in the D100%T sample is at a strain far beyond the yield strain, signifying that molecular chains had oriented along the deformation direction due to melting and recrystallization. Accordingly, the cavities in the D100%T system should align with their long axis along the deformation direction in order to comply with the orientation of molecular chains.

Focusing on the scattering patterns in each row from the die entrance toward the die exit, the cavitation intensity did not change in accordance with R_A^o. For the D25%T and D50%T samples, an enhancement of the scattering intensity occurred at first. But for positions approaching the die exit, the intensity decreased, and the scattering signals turned out to be similar to the ones for the die-drawn sample. To gain a better understanding of cavitation evolution, the Q value for each sample was calculated and is presented in Figure 7. The R_A^o dependence on distance from the corresponding position to the die entrance, *X* is also shown. Q values for the samples deformed by tensile stretching or die drawing are also included in Figure 7 for reference. As the tensile-stretched sample was not shaped by the die, the *X* value for this sample was set at 25 to assist with visibility of the data.

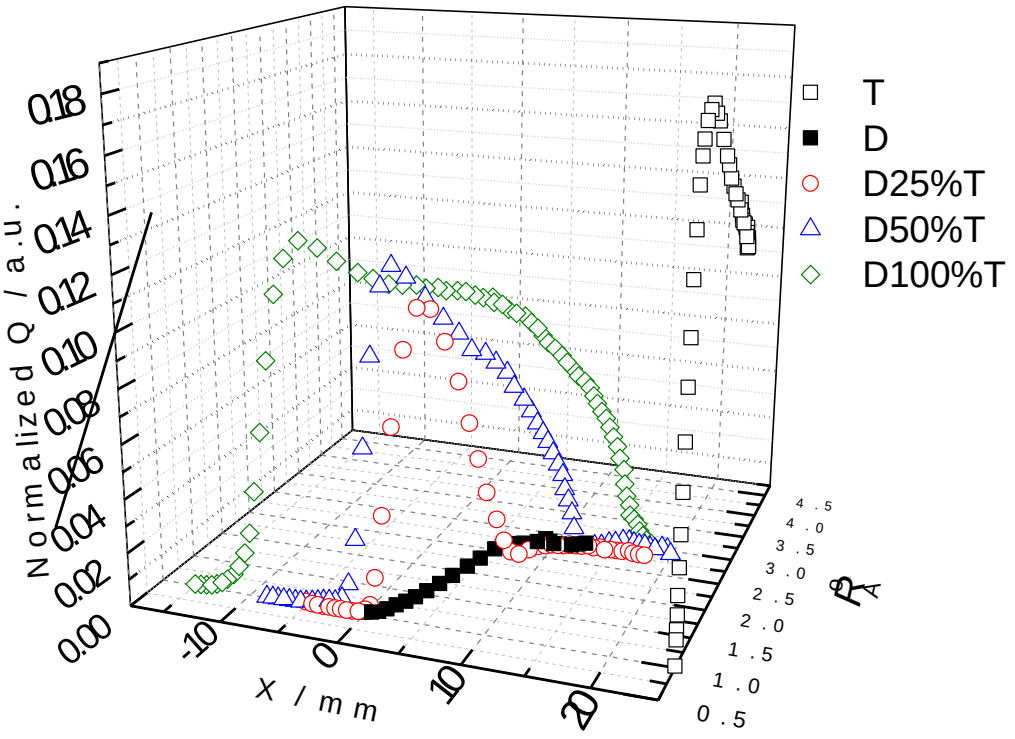

Figure 7. Normalized integrated scattering intensity of different samples as a function of draw ratio R_A^o, as well as the distance to the die entrance *X*.

For the sample deformed only via the die-drawing process, the starting data point was set at the corresponding position of the die entrance (*X*=0) on the sample (where no macroscopic deformation could be observed). Only a slight elevation of the Q could be found in the die-drawn sample. For the free tensile-stretched sample, not only did the Q value increase rapidly but also it reached a high level, as shown by the square hollow points in Figure 7. The Q changes clearly indicate that cavitation is significantly more intense in the tensile-stretched sample than the die-drawn one, which was consistent with the macroscopic appearance and the USAXS patterns of the deformed samples.

For the tensile-stretched sample, the early increase of Q before R_A^o=1.6 is attributed to newly-born cavities, and the growth of cavities. As for the following decrease at R_A^o beyond 1.6, it could not be interpreted as a result of the sample thinning during deformation, which is usually a main reason for a decrease in Q for a deformed sample,[36] since the scattering intensity was normalized. After the cavitation reaches a certain level, new cavities will not occur, instead the already-existing cavities will merge together, and the orientation of the cavities will also adjust. The gradually enlarged cavities might then be out of range of the USAXS technique. The volume occupied by these undetectable cavities would not be included in the cavity phase obtained by the USAXS technique and subsequently Q would slightly decrease since it is related to the volume fraction of the detectable cavities only. The Q values shown as circle, triangle, and diamond data points, which represented the results of the D25%T, D50%T, and D100%T samples, firstly increased and then decreased with R_A^o and *X*.

A peculiar phenomenon is the Q evolution of the undeformed part of the die drawing processed sample (including the part of the sample at the die entrance) during the second stage free stretching. In principle, the undeformed sample should go through the same path as the tensile-stretched sample, because, similar to the sample deformed via only the tensile-stretching process, this sample started with undeformed to deformed portions, then subjected to free tensile stretching. In practice, Q for this part of sample

did not follow the path observed for the tensile-stretched sample, especially for the D50%T and D100%T samples.

There might be two reasons for this. First of all, the micro-structure of the die-drawn sample near the die entrance may be disturbed[13, 37] during the die-drawing process, even though no macroscopic shape changing could be observed. This might lead to different deformation properties when this section was deformed during second stretching. Another possible reason is the necking process in the sample. As discussed above, necking would first occur somewhere between the die entrance and the die exit, then the neck would develop along the sample during second stage free stretching. In other words, the observed second free stretching induced deformation in the un-drawn section did not exhibit necking as abruptly as the tensile-stretched ones, since a relatively optimal deformation path had already been imposed on the samples during the die-drawing process.[13] Consequently, structure fragmentation is more severe in the tensile-stretched sample. This effect of the die-induced neck seemed to slowly decline as the sample was further stretched, as evidenced by the Q path evolution from the D25%T sample to the D100%T sample. The larger the extent of the second stage free stretching was, the closer the Q evolution path got to the result of the tensile-stretched sample.

More importantly, it is clear that most of the Q values of the D25%T, D50%T, and D100%T samples lay in between the ones for the samples deformed by either tensile stretching or die drawing. In our previous assumption, the nuclei of cavities should be

able to develop abruptly during a further stretching operation as a result of the lack of die confinement. Yet the observed Q of further stretched samples did not reach a comparable value to those for the tensile-stretched sample, indicating not many growable nuclei were preserved in the die-drawn samples. In other words, the die-drawing process did not suppress the cavitation phenomenon merely by hindering the growth of the cavities, it could also fundamentally diminish the amount of developable cavitation nuclei. The corresponding USAXS patterns and the evolution of Q of iPP stretched at 140 ºC during different deformation cases are described in Figure S2 and Figure S3 of the supporting information. They show a similar tendency to the results observed in Figure 6 and Figure 7, which further confirms that suppressed cavitation during die drawing is a general phenomenon.

3.3. Nucleation sites of the cavitation

There has been a long debate about where cavities are born in the first place during the deformation of a semi-crystalline polymer materials at small strains. [1, 3, 17, 38] Some believed the cavities originated from the amorphous phase, [1, 3] while others considered that the relatively weak connections between crystalline blocks within lamellae would lead to cavitation.[17, 38] These two theories were not entirely conflicting since the former is a model at the equatorial fan of the spherulites while the latter focusses on the lamellae with normals perpendicular to the external force.

Cavitation was definitely triggered during die drawing. However, more evidence is required to validate that new cavities were initiated during the second stage free tensile stretching of die drawn samples. Hence, the dimensions of the cavities of samples deformed via different routes were calculated based on the model proposed by Fischer *et al.*[31] This model does not precisely describe tilting cavities, subsequently the heights of these cavities (the length of axis along the deformation direction) could not be evaluated in the case of butterfly-like USAXS patterns. Thus, the heights of the cavities were not calculated until a capsule-like USAXS pattern appeared (e.g. for the D25%T sample, $R_{\mathrm{A}}^{\mathrm{o}}$=1.11 and for the tensile-stretched sample $R_{\mathrm{A}}^{\mathrm{o}}$=1.06). Some of the data points of the die-drawn sample were omitted since the scattering intensity was so weak that the data fitting was uncertain. The heights of the cavities were calculated and the results are presented in Figure 8, with error bars based on 95% confidence interval. The data points were also projected to the $R_{\mathrm{A}}^{\mathrm{o}}$-*X* plane (from Figure 5). Selected fitting curves using the Fischer's model are given in Figure S4 and the heights of cavities in iPP deformed at 140 ºC are recorded in Figure S5 of the supporting information.

For both the tensile-stretched sample and the die-drawn sample without second stage free stretching, the sizes of the cavities kept increasing with deformation level, indicating a better development of the cavities. For the D25%T, D50%T and D100%T samples the evolution of the size of cavities depended on $R_{\mathrm{A}}^{\mathrm{o}}$ and *X*. During the second stretching, the deformation of the die-drawn sample was accompanied by both the

development of the already existing cavities and the creation of new cavities. The development of the cavities increases the calculated average size, while the creation of new cavities decreases the average size of cavities. The competitive processes of both the development and the creation of cavities will affect the mean values of the height of cavities.

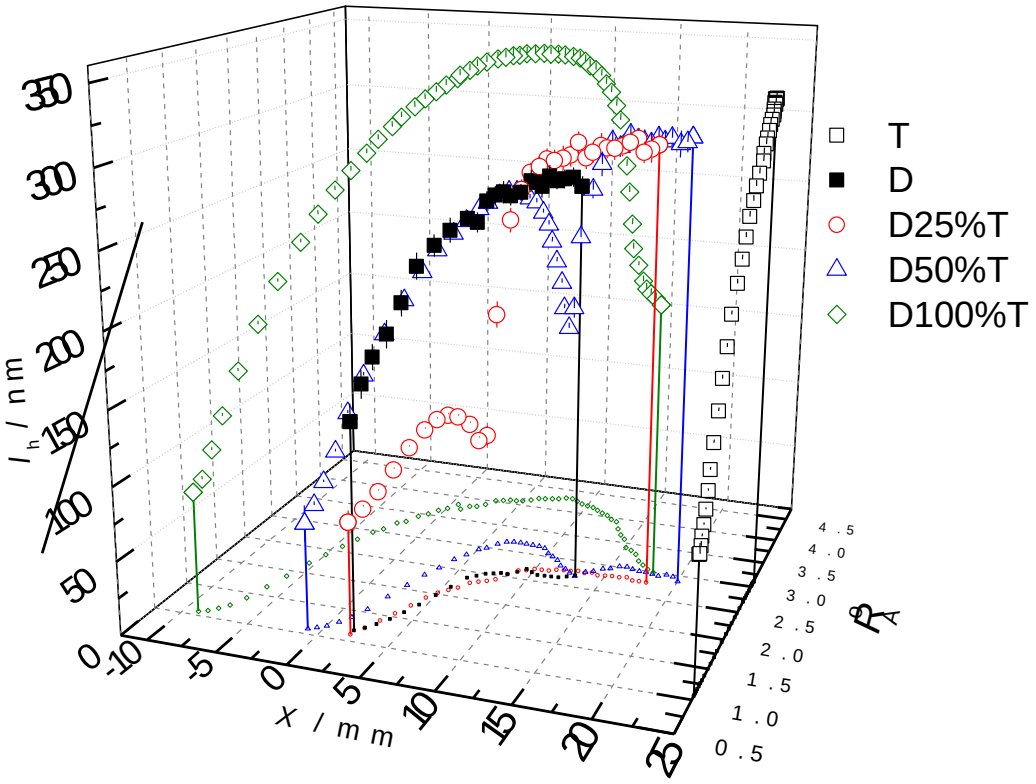

Figure 8. The size of cavities as a function of draw ratio R_A^o and distance to the die entrance position *X* of iPP samples during different deformation cases.

For the D25%T sample (circle points), the starting size of the cavities was smaller than for the die-drawn sample, indicating new cavities were initiated. After an initial increase, the sizes of the cavities decreased and then increased again, indicating that

formation of cavities prevailed at first, then the growth of the cavities prospered. When stretched to a larger degree (the D50%T sample, triangle points), the same behavior could be observed. As for the D100%T sample (diamond points), there was only a decrease after the initial increase of the size of the cavities. The evolution of the size of cavities in the undeformed part of the die-drawn samples exhibited similar features to the changes in Q during the second stage free stretching. The larger the second stage free stretching, the later the size of cavities deviated from the case of a sample deformed via only free tensile stretching. In addition, the development of the size of cavities in samples processed at 140 ºC was in line with the observation for 130 ºC deformation cases.

To confirm the heights of the cavities obtained using equation (4), SEM photos are shown in Figure 9 (SEM photos with a smaller magnification are shown in Figure S6 of the supporting information). The exact draw ratio of the sample parts observed in the SEM experiments was unavailable due to the random brittle fracture of the samples. It proved possible to obtain SEM photographs at two representative and distinguishable positions of each sample. SEM photographs Fig 9 (a), (c), and (f) were taken at positions around the die entrance while (b) and (d) were captured at positions close to the die exit. Since the $R_{\mathrm{A}}^{\mathrm{o}}$ of the D100%T sample at the die entrance was already large, the other SEM photo of this sample should be taken at a position possessing smaller $R_{\mathrm{A}}^{\mathrm{o}}$. In this case, photo (e) was taken at $R_{\mathrm{A}}^{\mathrm{o}}$ around 1.9($\pm$0.2). The dimensions of the observed

cavities in Figure 9 were close to the calculated ones based on the Fisher model using the USAXS data. Furthermore, the cavities appeared with their long axis perpendicular to the deformation direction in the D25%T sample while the ones occurred with their long axis parallel to the deformation direction in the D100%T sample at the positions with smaller $R_{\mathrm{A}}^{\mathrm{o}}$. The cavities in the D50%T sample expanded both along the perpendicular and the parallel directions at the position near the die entrance. However, all of the three samples had cavities with their long axis parallel to the deformation direction at locations with larger $R_{\mathrm{A}}^{\mathrm{o}}$. This agrees with the USAXS patterns shown in Figure 6.

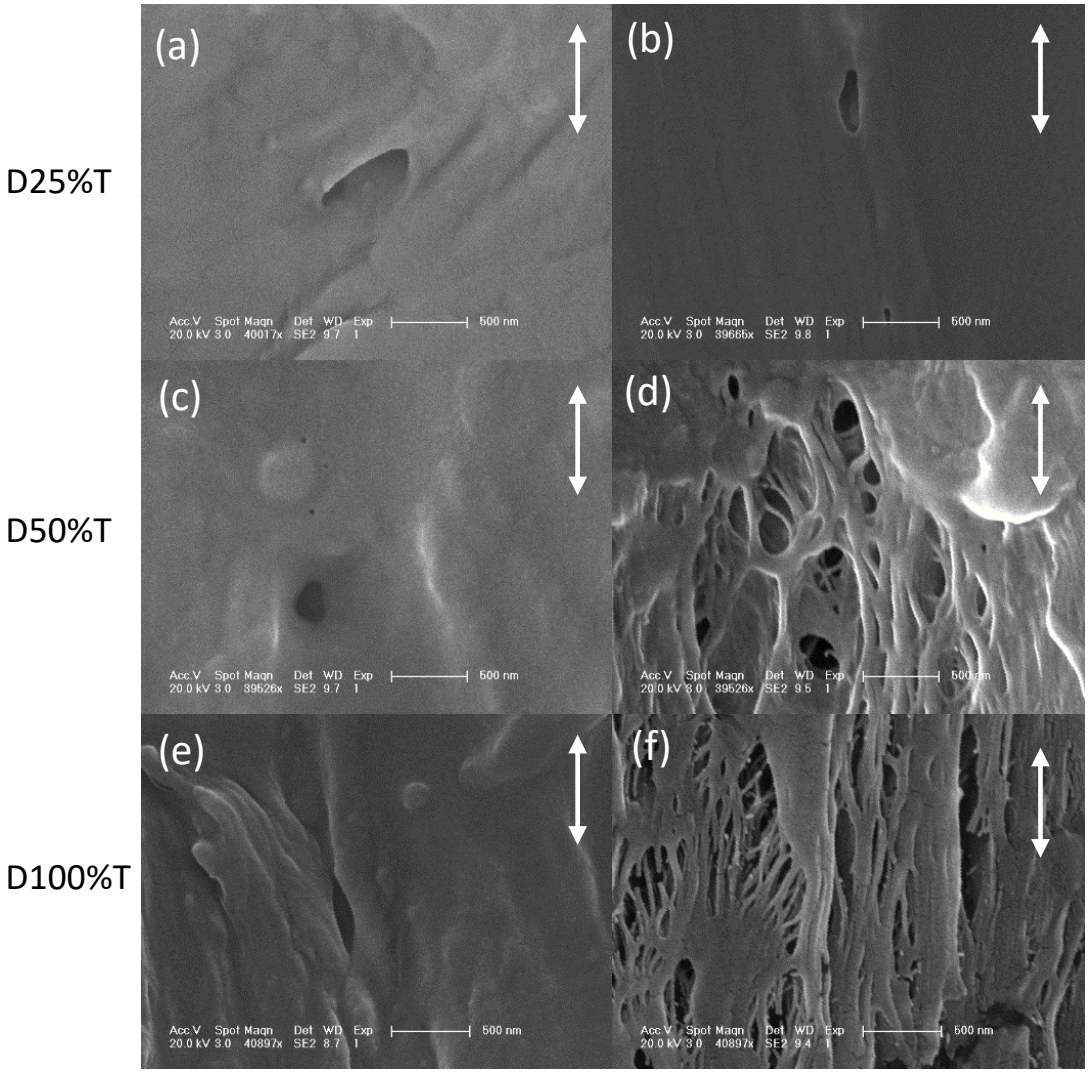

Figure 9. SEM photos of the D25%T, D50%T and D100%T samples. The arrows represented the elongation direction. (a), (c), and (f) were taken at positions around the die entrance, (b) and (d) were taken at positions closer to the die exit. (e) was taken at the position where the sample was not shaped by the die during the die-drawing process.

Clearly, new cavities were initiated during the second stage free tensile stretching. To investigate the nucleation sites of the cavities, a sample with only a slight deformation was investigated, to avoid overshadowing the new cavity nucleation

process by the development of existing cavities. Hence, the D25%T sample was chosen to assess cavitation behavior of a die-drawn sample during the second stage free tensile stretching. Selected USAXS patterns of a die-drawn sample and the D25%T sample are shown in Figure 10. Horizontal scattering streaks occurred at a low deformation in the second stage free tensile stretching, as evidenced by the USAXS patterns at the die entrance and exit positions. This indicates that the cavities which initiated during the second stage free tensile stretching were formed with their long axis perpendicular to the elongation direction.

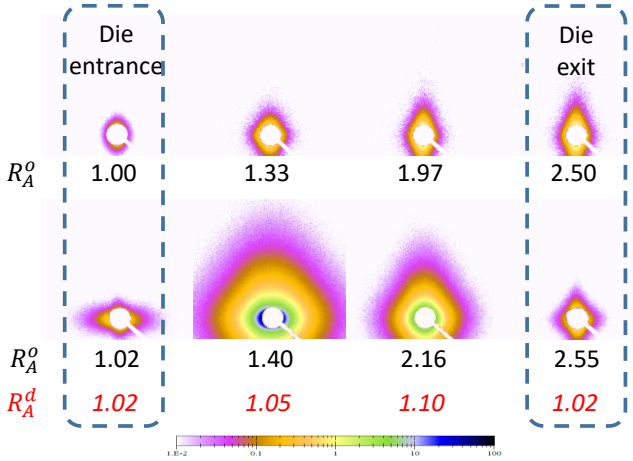

Figure 10. Selected USAXS patterns of the die-drawn sample (top) and the D25%T sample (bottom). Elongation direction: horizontal.

Another intriguing phenomenon is that the cavitation intensity is different at the die entrance and the die exit of the D25%T sample, even if a die-drawn sample is deformed to the same R_A^d at these positions. The evolution of cavitation before and after the second stage free tensile stretching (column 2 and 3 in Figure 10) is clear. Larger

cavitation intensity could be found in the column 2, even though a larger R_A^d was reached for the pattern in column 3. Q values for these locations are shown in Figure 7. All the experimental parameters that could influence the cavitation intensity were the same for these above-mentioned locations in the sample. Hence, the anomalous relationship between the cavitation intensity and R_A^d is assumed to originate from the different micro-structures at each position after the die-drawing process.

Compared with the α form, the β form of iPP was less stable and more likely to be fragmented during deformation. In order to understand the cavitation behavior at different locations in the die-drawn sample, it is helpful to focus on the evolution of the β form crystalline layers and the amorphous region in between. The β form lamellae along different directions could be evaluated by the intensity distribution along the $(300)_\beta$ diffraction ring, as shown in Figure 11. It was evident that the lamellae were not homogeneously distributed in the undeformed state (the black curve), indicating the existence of unevenly distributed daughter-parent lamellae of the β form iPP[39] induced by the injection molding process used to form the initial samples.[40]

With increasing deformation, the two peaks at -30° and 30° which originated from the daughter lamellae tend to merge together, while the position of the parent lamellae stay almost the same. The lamellae in the die-drawn samples can thus be divided into two sets: one set consists of the parent lamellae with their normal parallel to the elongation direction (designated as the parallel lamellae in the following discussion),

and the other set consists of lamellae with their normal approximately perpendicular to the elongation direction (designated as the perpendicular lamellae). The fractions of the perpendicular lamellae and the parallel lamellae were obtained by integrating the baseline-subtracted characteristic peaks. Considering the β phase lamellae would transform to the α phase lamellae, it is rational to further correct the above-mentioned fractions with the portions of the β phase at each position on the sample after the die-drawing process. The calculated values are shown in Figure 11.

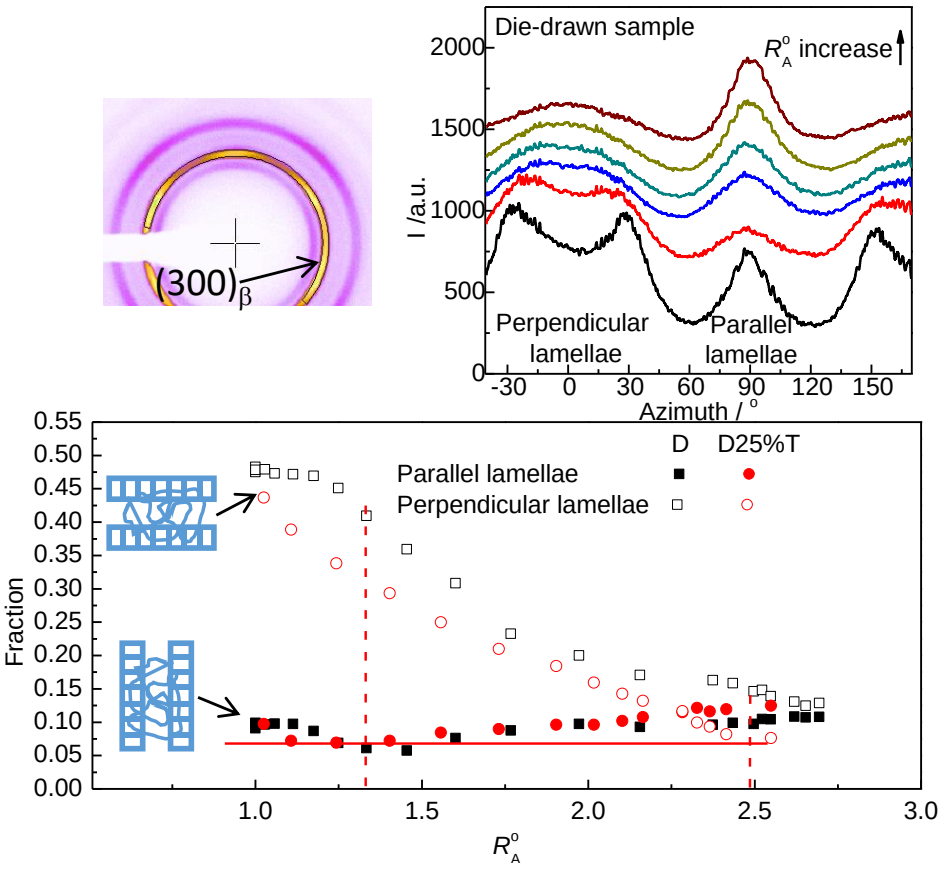

Figure 11. Top: The integral area on the 2D WAXD pattern of the $(300)_\beta$ diffraction ring and selected 1D integral curves of the die-drawn sample. Bottom: The evolution

of the β-form lamellae along different directions of the die-drawn sample (D) and the D25%T sample. Elongation direction: horizontal.

It is clear that the fractions of parallel lamellae in the die drawn sample do not further reduce after a decrease in the early stages of deformation (R_A^o<1.33), see Figure 11. On the contrary, the fractions of perpendicular lamellae kept decreasing beyond R_A^o=1.33. This suggests that the perpendicular lamellae as well as the amorphous region in between them should be responsible for the structure evolution and the phase transition during the second stage free tensile stretching.

From both the Q values in Figure 7 and the 2D USAXS patterns in Figure 10, sample locations beyond R_A^o=1.33 did not achieve cavitation intensity levels similar to those found in the less-deformed locations of the die-drawn sample, even when comparable or larger R_A^d values were reached during the second stage free tensile stretching. Apparently, the weakened cavitation capability can be linked to the decrease of the fraction of perpendicular lamellae and/or the amorphous region in between them. The fractions of the lamellae along different directions of the D25%T sample are also shown in Figure 11, from which it can be deduced that the perpendicular lamellae are fragmented during the second stage free tensile stretching.

In the previous discussion, the direction of the long axis of newly-born cavities was determined to be perpendicular to the elongation direction, based on the USAXS

patterns, i.e. the long axis of the cavities lies along the normal of the related lamellae. Hence, it seems to be more reasonable to suggest the cavities were born within the crystalline blocks inside the lamellae, perpendicular to the elongation direction during the second stage free tensile stretching.

Similar findings can be deduced for the cavitation behavior during the die-drawing process. Again, sample locations with relatively small deformation during die drawing are considered. The external force applied on the samples during the die-drawing process, including the drawing force as well as the compression and friction induced by the die, can be simplified into perpendicular and parallel forces, respectively.[27] The adjacent perpendicular lamellae will be pushed together by the die and the entity they form will be less sensitive to the external force. As was formulated by Galeski *et al.,* via a comparison between the yield stress (σ_y) and critical stress for cavitation (σ_{cav}) in a system, a phenomenological model suggests that cavitation occurs when $\sigma_y > \sigma_{cav}$. [3] The perpendicular lamellae are compressed during the die-drawing process. To reach the critical stress for triggering cavitation in these lamellae, an extra stress is needed to compensate the compression induced by the die walls. Therefore, a larger apparent critical stress for activation of cavitation is expected for the die-drawing process, comparing to free tensile stretching. Initiation of plastic flow is favored over the cavitation process in die drawing.

The suppression of cavitation in the die-drawing process is thus understood to be a consequence of reinforcing the connections between crystalline blocks in this process, subsequently diminishing the possibility of the initiation of cavitation within the perpendicular lamellae, due to an apparent increase of the critical stress for cavitation. In addition, these perpendicular lamellae could also be regarded as anchors of the polymer matrix at the beginning of deformation, confirmed by the almost unchanged fraction of these lamellae at the corresponding stage as shown in Figure 11. The parallel lamellae which firstly experience the β to α phase transition are expected to cause the local volume contraction due to the different densities of these two crystal forms.[20, 22] However, the volume contraction caused by the phase transition was constrained, as the parallel lamellae were surrounded by the fixed perpendicular lamellae. Using the results shown in Figure 3, the cavities born during the die-drawing process were large in size and aligned along the elongation direction as soon as they appeared. So the cavitation which took place in die drawing could be related to the local β to α transition of the parallel lamellae during deformation. More importantly, the cavitation during the die drawing is thought to be a collective activity of the parallel lamellae and their surrounded perpendicular lamellae rather than only the behaviour of parallel lamellae.

4. Conclusion

This work mainly focused on the cavitation behavior of a die-drawn sample. Three main issues can be summarized as follows. First, photographic evidence and 2D

USAXS patterns show that cavitation behavior is less intense in the die-drawn sample compared with a free tensile-stretched sample. The almost identical β to α phase transition behavior of the die-drawn sample and the free tensile-stretched sample indicate that the different cavitation behaviours observed is an outcome of the different routes of deformation rather than a result of the phase transition. Secondly, to investigate the physics behind the suppression of cavitation in die drawing process, USAXS scattering power (Q) and the sizes of the cavities were calculated. It was found that the die-drawing process fundamentally decreases the number of growable nuclei of cavities instead of merely confining the growth of the cavities. Thirdly, nucleation sites of the cavities have been identified. Different cavitation intensities were found at the different positions of the D25%T sample which was free tensile stretched to an overall deformation of 25% after die drawing. This cavitation intensity variation was successfully related to the lamellae fractions with normal perpendicular to the elongation direction during further free stretching. Together with the cavity directions, the nucleation sites are suggested to be within the crystalline layers. The reason for the decrease of the number of cavity-nuclei in the die drawing process is attributed to the elevated critical stress for cavitation, induced by the compressive stress perpendicular to the elongation direction exerted by the die wall.

ASSOCIATED CONTENT

Supporting Information. The macroscopic photos of iPP samples after different deformation cases, the fitting curves for calculating the heights of cavities using Fischer's model, the SEM photos of deformed iPP samples, and the USAXS patterns, the evolution of Q, as well as the heights of cavities of iPP during different deformation processes at 140 ºC.

AUTHOR INFORMATION

Corresponding Author

*E-mail: luying@ciac.ac.cn. (Y. L.)

*E-mail: men@ciac.ac.cn. (Y. M.)

Funding Sources

This work is supported by the National Natural Science Foundation of China (21704102 and 51525305), Newton Advanced Fellowship of the Royal Society, United Kingdom (NA 150222) and ExxonMobil.

Notes

The authors declare no competing financial interest.

ACKNOWLEDGMENT

The authors thank Prof. Lifeng Wang at Jilin University for his kindly assistance on the free tensile-stretching experiments. The authors thank Associate Prof. Meiye Li at CIAC for her kindly assistance on the ESEM experiments.

REFERENCES

(1) Pawlak, A.; Galeski, A.; Rozanski, A. Cavitation During Deformation of Semicrystalline Polymers. *Prog. Polym. Sci.* **2014**, *39*, 921-958.

(2) Lu, Y.; Wang, Y.; Chen, R.; Zhao, J.; Jiang, Z.; Men, Y. Cavitation in Isotactic Polypropylene at Large Strains During Tensile Deformation at Elevated Temperatures. *Macromolecules* **2015**, *48*, 5799-5806.

(3) Pawlak, A.; Galeski, A. Plastic Deformation of Crystalline Polymers: The Role of Cavitation and Crystal Plasticity. *Macromolecules* **2005**, *38*, 9688-9697.

(4) Blaise, A.; Baravian, C.; Andre, S.; Dillet, J.; Michot, L. J.; Mokso, R. Investigation of the Mesostructure of a Mechanically Deformed HDPE by Synchrotron Microtomography. *Macromolecules* **2010**, *43*, 8143-8152.

(5) Lyu, D.; Chen, R.; Lu, Y.; Men, Y. Subsequent but Independent Cavitation Processes in Isotactic Polypropylene During Stretching at Small- and Large-Strain Regimes. *Ind. Eng. Chem. Res.* **2018**, *57*, 8927-8937.

(6) Wei, P. D.; Huang, J. C.; Lu, Y.; Zhong, Y.; Men, Y. F.; Zhang, L. N.; Cai, J. Unique Stress Whitening and High-Toughness Double-Cross-Linked Cellulose Films. *ACS Sustain. Chem. Eng.* **2019**, *7*, 1707-1717.

(7) Arora, P.; Zhang, Z. Battery Separators. *Chem. Rev.* **2004**, *104*, 4419-4462.

(8) Lei, C. H.; Xu, R. J.; Tian, Z. Q.; Huang, H. H.; Xie, J. Y.; Zhu, X. Q. Stretching-Induced Uniform Micropores Formation: An in Situ SAXS/WAXD Study. *Macromolecules* **2018**, *51*, 3433-3442.

(9) Wu, G. G.; Chen, W. B.; Ding, C.; Xu, L. Y.; Liu, Z. Y.; Yang, W.; Yang, M. B. Pore Formation Mechanism of Oriented Beta Polypropylene Cast Films During Stretching and Optimization of Stretching Methods: In-Situ SAXS and WAXD Studies. *Polymer* **2019**, *163*, 86-95.

(10) Oliviero, M.; Verdolotti, L.; Stanzione, M.; Lavorgna, M.; Iannace, S.; Tarello, M.; Sorrentino, A. Bio-Based Flexible Polyurethane Foams Derived from Succinic Polyol: Mechanical and Acoustic Performances. *J. Appl. Polym. Sci.* **2017**, *134*, 45113.

(11) Zhang, X. L.; Wang, X. H.; Sun, B. J.; Cheng, H. R.; Chen, J. B.; Shen, C. Y.; Park, C. B. Broadened Foaming Scope of iPP Adjusted by Its Self-Enhancement and Nucleating Agent under Compressed CO_2. *Mater. Today Commun.* **2018**, *17*, 501-510.

(12) Lee, P. C.; Kaewmesri, W.; Wang, J.; Park, C. B.; Pumchusak, J.; Folland, R.; Praller, A. Effect of Die Geometry on Foaming Behaviors of High-Melt-Strength Polypropylene with CO_2. *J. Appl. Polym. Sci.* **2008**, *109*, 3122-3132.

(13) Coates, P. D.; Caton-Rose, P.; Ward, I. M.; Thompson, G. Process Structuring of Polymers by Solid Phase Orientation Processing. *Sci. China Chem.* **2013**, *56*, 1017-1028.

(14) Dijkstra, P. T. S.; Van Dijk, D. J.; Huetink, J. A Microscopy Study of the Transition from Yielding to Crazing in Polypropylene. *Polym. Eng. Sci.* **2002**, *42*, 152-160.

(15) Humbert, S.; Lame, O.; Chenal, J. M.; Rochas, C.; Vigier, G. New Insight on Initiation of Cavitation in Semicrystalline Polymers: In-Situ SAXS Measurements. *Macromolecules* **2010**, *43*, 7212-7221.

(16) Jiang, Z.; Chen, R.; Lu, Y.; Whiteside, B.; Coates, P.; Wu, Z.; Men, Y. Crystallization Temperature Dependence of Cavitation and Plastic Flow in the Tensile Deformation of Poly(Epsilon-Caprolactone). *J. Phys. Chem. B* **2017**, *121*, 6673-6684.

(17) Lu, Y.; Men, Y. F. Cavitation-Induced Stress Whitening in Semi-Crystalline Polymers. *Macromol. Mater. Eng.* **2018**, *303*, 1800203.

(18) Aboulfaraj, M.; Gsell, C.; Ulrich, B.; Dahoun, A. In-Situ Observation of the Plastic Deformation of Polypropylene Spherulites under Uniaxial Tension and Simple Shear in the Scanning Electron-Microscope. *Polymer* **1995**, *36*, 731-742.

(19) Lezak, E.; Bartczak, Z.; Galeski, A. Plastic Deformation Behavior of Beta-Phase Isotactic Polypropylene in Plane-Strain Compression at Room Temperature. *Polymer* **2006**, *47*, 8562-8574.

(20) Chu, F.; Yamaoka, T.; Kimura, Y. Crystal Transformation and Micropore Formation During Uniaxial Drawing of Beta-Form Polypropylene Film. *Polymer* **1995**, *36*, 2523-2530.

(21) Varga, J. Beta-Modification of Isotactic Polypropylene: Preparation, Structure,

Processing, Properties, and Application. *J. Macromol. Sci. Phys.* **2002**, *B41*, 1121-1171.

(22) Chu, F.; Yamaoka, T.; Ide, H.; Kimura, Y. Microvoid Formation Process During the Plastic-Deformation of Beta-Form Polypropylene. *Polymer* **1994**, *35*, 3442-3448.

(23) Coates, P. D.; Ward, I. M. Die Drawing: Solid-Phase Drawing of Polymers through a Converging Die. *Polym. Eng. Sci.* **1981**, *21*, 612-618.

(24) Li, J. F.; Li, Z. Q.; Ye, L.; Zhao, X. W.; Coates, P.; Caton-Rose, F.; Martyn, M. Structure Evolution and Orientation Mechanism of Long-Chain-Branched Poly (Lactic Acid) in the Process of Solid Die Drawing. *Eur. Polym. J.* **2017**, *90*, 54-65.

(25) Vgenopoulos, D.; Sweeney, J.; Grant, C. A.; Thompson, G. P.; Spencer, P. E.; Caton-Rose, P.; Coates, P. D. Nanoindentation Analysis of Oriented Polypropylene: Influence of Elastic Properties in Tension and Compression. *Polymer* **2018**, *151*, 197-207.

(26) Taraiya, A. K.; Richardson, A.; Ward, I. M. Production and Properties of Highly Oriented Polypropylene by Die Drawing. *J. Appl. Polym. Sci.* **1987**, *33*, 2559-2579.

(27) Lyu, D.; Sun, Y.; Thompson, G.; Lu, Y.; Caton-Rose, P.; Lai, Y.; Coates, P.; Men, Y. Die Geometry Induced Heterogeneous Morphology of Polypropylene inside the Die During Die-Drawing Process. *Polym. Test.* **2019**, *74*, 104-112.

(28) Lu, Y.; Lyu, D.; Cavallo, D.; Men, Y. Enhanced Beta to Alpha Recrystallization in Beta Isotactic Polypropylene with Different Thermal Histories. *Polym. Cryst.* **2019**, *2*, e10040.

(29) Somani, R. H.; Hsiao, B. S.; Nogales, A.; Fruitwala, H.; Srinivas, S.; Tsou, A. H. Structure Development During Shear Flow Induced Crystallization of i-PP: In Situ Wide-Angle X-Ray Diffraction Study. *Macromolecules* **2001**, *34*, 5902-5909.

(30) Porod, G. In Small-Angle X-ray Scattering; Glatter, O., Kratky, O., Eds.; Academic Press: New York, 1982; p 35.

(31) Fischer, S.; Diesner, T.; Rieger, B.; Marti, O. Simulating and Evaluating Small-Angle X-Ray Scattering of Micro-Voids in Polypropylene During Mechanical Deformation. *J. Appl. Crystallogr.* **2010**, *43*, 603-610.

(32) Bao, R. Y.; Ding, Z. T.; Liu, Z. Y.; Yang, W.; Xie, B. H.; Yang, M. B. Deformation-Induced Structure Evolution of Oriented Beta-Polypropylene During Uniaxial Stretching. *Polymer* **2013**, *54*, 1259-1268.

(33) Zhang, C. B.; Liu, G. M.; Song, Y.; Zhao, Y.; Wang, D. J. Structural Evolution of Beta - iPP During Uniaxial Stretching Studied by in-Situ WAXS and SAXS. *Polymer* **2014**, *55*, 6915-6923.

(34) Cai, Z.; Zhang, Y.; Li, J.; Xue, F.; Shang, Y.; He, X.; Feng, J.; Wu, Z.; Jiang, S. Real Time Synchrotron Saxs and Waxs Investigations on Temperature Related Deformation and Transitions of β-iPP with Uniaxial Stretching. *Polymer* **2012**, *53*, 1593-1601.

(35) Lu, Y.; Men, Y. F. Initiation, Development and Stabilization of Cavities During Tensile Deformation of Semicrystalline Polymers. *Chinese J. Polym. Sci.* **2018**, *36*,

1195-1199.

(36) Wang, Y.; Jiang, Z.; Fu, L.; Lu, Y.; Men, Y. Lamellar Thickness and Stretching Temperature Dependency of Cavitation in Semicrystalline Polymers. *Plos One* **2014**, *9,* e97234.

(37) Motashar, F. A.; Unwin, A. P.; Craggs, G.; Ward, I. M. Analytical and Experimental-Study of the Die Drawing of Circular Rods through Conical Dies. *Polym. Eng. Sci.* **1993**, *33*, 1288-1298.

(38) Men, Y. F.; Rieger, J.; Homeyer, J. Synchrotron Ultrasmall-Angle X-Ray Scattering Studies on Tensile Deformation of Poly(1-Butene). *Macromolecules* **2004**, *37*, 9481-9488.

(39) Liu, Z. Z.; Liu, X. H.; Zheng, G. Q.; Dai, K.; Liu, C. T.; Shen, C. Y.; Yin, R.; Guo, Z. H. Mechanical Enhancement of Melt-Stretched Beta-Nucleated Isotactic Polypropylene: The Role of Lamellar Branching of Beta-Crystal. *Polym. Test.* **2017**, *58*, 227-235.

(40) Kantz, M. R.; Newman, H. D.; Stigale, F. H. The Skin-Core Morphology and Structure-Property Relationships in Injection-Molded Polypropylene. *J. Appl. Polym. Sci.* **1972**, *16*, 1249-1260.

Suppressed cavitation in die-drawn isotactic polypropylene

Dong Lyu,[1,2] Yingying Sun,[3] Ying Lu,[1,] Lingzhi Liu,[1] Ran Chen,[1] Glen Thompson,[4]*

Philip Caton-Rose,[4] Phil Coates,[4] Yan Wang,[5] Yongfeng Men.[1,2,]*